

Time-Varying Graph Learning with Constraints on Graph Temporal Variation

Koki Yamada, *Student Member, IEEE*, Yuichi Tanaka, *Senior Member, IEEE*, and Antonio Ortega, *Fellow, IEEE*

Abstract—We propose a novel framework for learning time-varying graphs from spatiotemporal measurements. Given an appropriate prior on the temporal behavior of signals, our proposed method can estimate time-varying graphs from a small number of available measurements. To achieve this, we introduce two regularization terms in convex optimization problems that constrain sparseness of temporal variations of the time-varying networks. Moreover, a computationally-scalable algorithm is introduced to efficiently solve the optimization problem. The experimental results with synthetic and real datasets (point cloud and temperature data) demonstrate our proposed method outperforms the existing state-of-the-art methods.

Index Terms—Graph learning, time-varying graph, topology identification, network inference, dynamic graph.

I. INTRODUCTION

SIGNALS often have underlying network structures, e.g., sensor, traffic, brain, and social networks. Graphs, consisting of sets of nodes and edges, are a fundamental tool to describe the relationship among entities. Graph edges and the corresponding edge weights can be used to capture the similarity between nodes (where a higher positive weight indicates greater similarity). Introducing a graph representation enables us to efficiently analyze signals on networks in many practical applications such as epidemics [1], [2], transportation networks [3], and social networks [4].

Even when data is not associated with an actual network, graphs are efficient tools to represent latent structures in the data. For example, a principal component analysis can be improved by imposing a prior based on graphs [5]–[7]. Graph-based image processing enables us to improve performance in several image processing tasks [8]–[13]. However, graphs are not provided in many cases *a priori*.

Graph learning methods aim at identifying graphs from observed data [14]–[16]. Each observation is a vector, and each entry corresponds to the observation at one node. The goal is to obtain the weights of all the edges connecting those nodes. Most graph learning methods identify a single static graph from all the observations [17]–[25]. These *static graph learning* methods assume that the node relationships obtained from the observations do not change during the measurement

process. However, in many applications where the observations are obtained over a period of time, a time-varying graph will provide a better model. Examples of such applications include estimation of the time-varying brain functional connectivity from EEG or fMRI data [26], identification of temporal transit of biological networks such as protein, RNA, and DNA [27], and inference of relationships among companies from historical stock price data [28], dynamic point cloud processing, and analysis of physical measurement data such as temperature. A straightforward approach to estimate a time-varying graph would consist of aggregating temporal observations into non-overlapping windows and then using an existing static graph learning method to estimate a graph for each time windows. However, such an approach would possess some drawbacks.

First, this method would estimate a graph *independently* for each temporal interval, thus ignoring temporal relations that may exist in time-varying graphs. Second, time-varying graph learning may require estimating graphs from time windows containing only a small fraction of observations due to the trade-off between the choice of window length and temporal resolution. For example, if we choose a short window to adapt to fast temporal changes in the graph, then we may not have enough data to learn a graph within each window. However, the existing static graph learning methods, however, cannot successfully infer graphs from a small number of observations. On the other hand, if we use a longer window, we may not be able to keep up with the temporal changes.

This paper presents a *time-varying graph learning* method based on time-varying graph factor analysis (TGFA), which is an extension of its static counterpart, static graph factor analysis (SGFA) [18]. We propose the TGFA-based methods to estimate time-varying graphs from a collection of spatiotemporal measurements. The SGFA formulates a signal generation model based on a graph signal processing (GSP) perspective, where it is assumed that the observed signals have some specific spectral properties with respect to graph Fourier transform (GFT) of the graph to be learned. For example, if a multivariate Gaussian model is chosen, it leads to observed signals generated from a Gaussian distribution whose inverse covariance matrix (i.e., precision matrix) is given by the graph Laplacian of the underlying graph [14], [18]. Unlike SGFA, TGFA considers the graph evolution as illustrated in Fig. 1. The graph evolution can be represented by a sequence of graph Laplacians and their corresponding temporal variations.

This study focuses on two time-varying graph models, with the following two properties:

(P1) Temporal homogeneity: Most edges and their weights in the time-varying graph should remain unchanged over a

K. Yamada is with the Graduate School of BASE, Tokyo University of Agriculture and Technology, Tokyo 184-8588, Japan (e-mail: k-yamada@msp-lab.org).

Y. Tanaka is with the Graduate School of BASE, Tokyo University of Agriculture and Technology, Tokyo 184-8588, Japan, and also with the PRESTO, Japan Science and Technology Agency, Kawaguchi 332-0012, Japan (e-mail: ytnk@cc.tuat.ac.jp).

A. Ortega is with the Department of Electrical and Computer Engineering, University of Southern California, Los Angeles, CA 90089 USA (antonio.ortega@sipi.usc.edu).

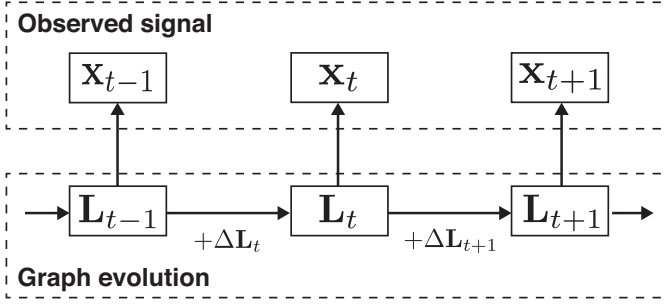


Fig. 1. An overview of time-varying graph factor analysis. L_t and ΔL_t represent the graph Laplacian at the t th time slot and the graph temporal variation. This study focuses on learning a time-varying graph, which is the sequence of the graph Laplacian, from the observed signal \mathbf{x} .

short-term time horizon. In other words, at any given time only a small number of edges in time-varying graphs change. Time-varying graphs in many applications satisfy this property. For example, consider a sensor network where the nodes and the edges represent sensor locations and correlations among sensor measurements respectively. If the sensors record the temperature in a building, various factors such as air conditioning, sunlight, and number of people in the room, locally affect the correlations among the sensor measurements but these factors vary smoothly over time. As a result, this sensor network will be a time-varying graph such that most edges remain constant, while the weights change only slightly over time, i.e., it follows (P1). In addition to this example, time-varying graphs in fMRI and various biological networks seem to have this property [27], [29].

(P2) Switching behavior: Edges and weights remain almost unchanged over time; however, they may suddenly change within a few time slots. This type of time-varying graph appears in situations where some factors cause sudden changes in graph topologies. Prominent examples include brain networks, where epileptic seizures make their topology change suddenly [30].

In this paper, we design an algorithm to estimate the two types of time-varying graphs, namely, graphs with temporal homogeneity and graphs with switching behavior. For this purpose, we formulate the graph learning problem as a convex optimization with regularization of temporal variation derived from TGFA. To solve the convex optimization problem, we utilize a primal-dual splitting algorithm [31], which enables us to estimate time-varying graphs more successfully than static graph learning methods.

In experiments with synthetic datasets, our proposed method outperforms existing methods especially when only small amounts of data are available. We also evaluate the performance of our methods for tasks involving real data, such as dynamic point cloud denoising and learning time-varying graphs from spatiotemporal meteorological and temperature data. Our results for dynamic point cloud denoising show that the estimating graph topology information with our method allows us to improve the denoising performance. In the meteorological and temperature data application, we show that our method can learn reasonable time-varying graphs that capture the geographical characteristics *without using geographical*

information. Our recent work [32] proposed a framework for learning time-varying graphs that follow (P1). Our work in this paper substantially extends the work in [32] by allowing learning for graphs with property (P2), which is more suitable for change point detection problems. We also evaluate the robustness of our proposed approach under several conditions of temporal resolution and we compare the computation time with some related approaches.

The remainder of this paper is organized as follows. Section II presents preliminaries concerning graphs and proximal operators. Section III describes the problem formulation of time-varying graph learning. Section IV defines the regularization for temporal graph variation and the optimization problem to learn graphs and proposes an algorithm to find a solution. Section V and VI provides experimental results with synthetic data and real data respectively. Finally, we show the conclusion and future works of this study in Section VII.

A. Related Work

Several approaches address graph learning problem, and two overview papers about graph learning have been published recently [14], [15]. Among the techniques for learning time-varying graphs, the Kalofolias et al. method, where constraints are introduced so that the edge weights change smoothly over time, is close to ours [33]. This approach uses a smoothness criterion and Tikhonov regularization of temporal variation in graphs to learn a time-varying graph. However, it does not learn time-varying graphs following (P1) exactly because Tikhonov regularization promotes smooth variation of edge weights over time, i.e., it allows changes of both edges and edge weights over short-term time horizons. While our approach has similar cost functions as those employed in [33], we use different regularization terms that favors learning time-varying graphs with the (P1) property. However, we cannot solve the optimization problem in our approach straightforwardly in the same manner as [33] because the regularization terms used are not differentiable. Therefore, we reformulate the optimization problem to make it solvable with a primal-dual splitting algorithm that leads to an efficient learning of a time-varying graph.

Hallac et al. addresses the problem of learning a time-varying graph using time-varying graphical Lasso (TVGL) [28], which combines graphical Lasso with a temporal regularization and finds the solution using alternating direction method of multipliers (ADMM). Note that graphs estimated with this approach often have negative edge weights. In contrast, our proposed method constrains to have non-negative edges in the estimated graph, because such graphs are often desired for many applications [14], [15]. Furthermore, our method has a lower computation complexity, as TVGL requires eigendecompositions of target matrices to calculate a proximal operator of a logarithm determinant term, whereas our approach is an eigendecomposition-free algorithm.

Baigana et al. consider the problem of identifying a time-varying graph to capture causal relationships in the network contagion evolution [34]. This model focuses on the spread process on networks (e.g., infectious diseases and fake news)

TABLE I
LIST OF NOTATION

N	Number of nodes
K	Number of data chunk
T	Number of time frames
$a_i, (\mathbf{a})_i, a[i]$	i th entry of a vector
$A_{ij}, (\mathbf{A})_{ij}$	(i, j) entry of a matrix
$(\mathbf{A})_i$	i th column of \mathbf{A}
\mathbf{A}^\dagger	Moore-Penrose pseudoinverse of \mathbf{A}
\mathbb{R}_+	Set of the nonnegative real numbers
\circ	Hadamard product
$\ \mathbf{a}\ _2^2, \ \mathbf{A}\ _F^2$	sum of squared values of all elements
$\ \mathbf{a}\ _1, \ \mathbf{A}\ _1$	sum of absolute values of all elements
$\text{Tr}(\mathbf{A})$	Trace of a matrix
$\text{diag}(\mathbf{A})$	vector formed by diagonal elements

and aims to identify the links propagating information over nodes at each time. However, only directed graphs can be estimated by this approach. In contrast, our method estimates undirected graphs whose connections change over time. This is often desired for data that do not have causal relationships. For example, data acquired by physical sensors such as point cloud coordinates and temperatures.

B. Notation

The notation used in this paper is summarized in Table I. Throughout this paper, vectors and matrices are written in bold lowercase and bold uppercase letters respectively. The calligraphic capital letters, namely, \mathcal{V} and \mathcal{W}_m , denote sets.

II. PRELIMINARIES

A. Basic Definitions for GSP

An undirected weighted graph is represented as $\mathcal{G} = (\mathcal{V}, \mathcal{E}, \mathbf{W})$, where \mathcal{V} is a set of nodes, \mathcal{E} is a set of edges, and \mathbf{W} is a weighted adjacency matrix. The number of nodes is given by $N = |\mathcal{V}|$. Each element of the weighted adjacency matrix is defined by

$$(\mathbf{W})_{mn} = \begin{cases} w_{mn} & \text{if nodes } m \text{ and } n \text{ are connected,} \\ 0 & \text{otherwise,} \end{cases} \quad (1)$$

where $w_{mn} \geq 0$ is the edge weight between nodes m and n . The degree matrix \mathbf{D} is a diagonal matrix whose diagonal element is $d_{mm} = \sum_n w_{mn}$. The graph Laplacian is given by $\mathbf{L} = \mathbf{D} - \mathbf{W}$. Let $\mathbf{f} \in \mathbb{R}^N$ be a signal on the graph, then the Laplacian quadratic form is given by

$$\mathbf{f}^\top \mathbf{L} \mathbf{f} = \frac{1}{2} \sum_{m,n} w_{mn} (f_m - f_n)^2, \quad (2)$$

where f_m and f_n denote the signal values at nodes m and n , respectively. Note that (2) provides a smoothness measure of the signal on the graph [35].

Since \mathbf{L} is a real symmetric matrix, it has orthogonal eigenvectors and can be decomposed into $\mathbf{L} = \mathbf{U} \mathbf{\Lambda} \mathbf{U}^\top$, where $\mathbf{U} = [\mathbf{u}_0, \mathbf{u}_1, \dots, \mathbf{u}_{N-1}]$ is a matrix whose i -th column is the eigenvector \mathbf{u}_i and $\mathbf{\Lambda} = \text{diag}(\lambda_0, \lambda_1, \dots, \lambda_{N-1})$ is a diagonal

eigenvalue matrix. The graph Fourier transform (GFT) and the inverse GFT are defined as

$$\hat{f}[i] = \langle \mathbf{u}_i, \mathbf{f} \rangle = \sum_{n=0}^{N-1} u_i[n] f[n], \quad (3)$$

$$f[n] = \sum_{i=0}^{N-1} \hat{f}[i] u_i[n]. \quad (4)$$

Eigenvalues of the graph Laplacian correspond to frequencies in the classical Fourier transform, and thus, are often called *graph frequencies*.

B. Proximal Operator and Its Properties

Let $f : \mathbb{R}^n \rightarrow \mathbb{R} \cup \{\infty\}$ be a proper lower semicontinuous convex function. The proximal operator $\text{prox}_{\gamma f} : \mathbb{R}^n \rightarrow \mathbb{R}^n$ of f with a parameter $\gamma > 0$ is defined by

$$\text{prox}_{\gamma f}(\mathbf{x}) = \arg \min_{\mathbf{y}} f(\mathbf{y}) + \frac{1}{2\gamma} \|\mathbf{y} - \mathbf{x}\|_2^2. \quad (5)$$

If a proximal operator $\text{prox}_{\gamma f}$ can be computed efficiently, the function f is called proximal.

Proximal operators have the following properties [36]:

- If a function f is separable across variables, i.e., $f(\mathbf{x}) = f_1(\mathbf{x}_1) + f_2(\mathbf{x}_2)$ with $\mathbf{x} = [\mathbf{x}_1^\top \mathbf{x}_2^\top]^\top$, then

$$\text{prox}_{\gamma f}(\mathbf{v}) = [(\text{prox}_{\gamma f_1}(\mathbf{v}_1))^\top (\text{prox}_{\gamma f_2}(\mathbf{v}_2))^\top]^\top, \quad (6)$$

where $\mathbf{v} = [\mathbf{v}_1^\top \mathbf{v}_2^\top]^\top$. Thus, the computation in the proximal operator of separable functions reduces to the computation of the proximal operator for each separable part.

- If a function f is fully separable, i.e., $f(\mathbf{x}) = \sum_i f_i(x_i)$, then

$$(\text{prox}_{\gamma f}(\mathbf{v}))_i = \text{prox}_{\gamma f_i}(v_i). \quad (7)$$

Therefore, in this case, the computation of proximal operator can be reduced to the elementwise computation.

III. PROBLEM FORMULATION FOR TIME-VARYING GRAPH LEARNING

We first describe the static graph factor analysis (SGFA) [18], which introduces a model for the generation of graph signals. Subsequently, we introduce a time-varying graph factor analysis (TGFA), which extends SGFA to formulate the time-varying graph learning problems studied in this paper.

A. Static Graph Factor Analysis

The observation model of SGFA is defined as follows [18]:

$$\mathbf{x} = \mathbf{U} \mathbf{h} + \boldsymbol{\epsilon}, \quad (8)$$

where $\mathbf{x} \in \mathbb{R}^N$ is an observed signal, $\mathbf{h} \in \mathbb{R}^N$ is a latent variable represented in the graph frequency domain, \mathbf{U} is the GFT matrix and $\boldsymbol{\epsilon} \sim \mathcal{N}(0, \sigma_\epsilon^2 \mathbf{I})$ is an additive white Gaussian noise. The observation model in (8) means that the signals possessing graph structures can be represented by the inverse GFT of latent variables in the spectral domain of the

underlying graph. SGFA assumes that the latent variable \mathbf{h} follows the multivariate Gaussian distribution

$$p(\mathbf{h}) = \mathcal{N}(0, \mathbf{A}^\dagger). \quad (9)$$

This corresponds to the assumption, that signal energy tends to be concentrated in the low frequencies and thus encourages graph signal smoothness. Equations (8) and (9) lead to the conditional probability of \mathbf{x} given \mathbf{h} :

$$p(\mathbf{x}|\mathbf{h}) = \mathcal{N}(\mathbf{U}\mathbf{h}, \sigma_\epsilon^2 \mathbf{I}). \quad (10)$$

From (9) and (10), the marginal distribution of \mathbf{x} is given by:

$$p(\mathbf{x}) = \mathcal{N}(0, \mathbf{L}^\dagger + \sigma_\epsilon^2 \mathbf{I}). \quad (11)$$

Note that the fact $\mathbf{L}^\dagger = \mathbf{U}\mathbf{A}^\dagger\mathbf{U}^\top$ is used in the derivation of (11). The marginal distribution in (11) indicates that a graph signal \mathbf{x} can be generated by the degenerate multivariate Gaussian distribution whose precision matrix is the graph Laplacian of the underlying graph. The maximum a posteriori estimation of \mathbf{h} leads to the following problem:

$$\min_{\mathbf{L}, \mathbf{y}} \|\mathbf{x} - \mathbf{y}\|_2^2 + \alpha \mathbf{y}^\top \mathbf{L} \mathbf{y}, \quad (12)$$

where $\mathbf{y} = \mathbf{U}\mathbf{h}$ and \mathbf{y} is regarded as a noiseless signal. If the observed signal \mathbf{x} is noise-free, this optimization problem finds the graph Laplacian that minimizes the smoothness measure as in (2).

B. Time-varying Graph Factor Analysis

Suppose that we have a multivariate time series data divided with non-overlapping time windows $\{\mathbf{X}_1, \dots, \mathbf{X}_T\}$, where $\mathbf{X}_t = [\mathbf{x}_1^{(t)}, \dots, \mathbf{x}_K^{(t)}] \in \mathbb{R}^{N \times K}$ contains K observations at a time window t , and the graph corresponding to observations in the same time window is invariant. The choice of K depends on a sampling frequency in measurements. Our goal is to learn a sequence of graph Laplacians $\mathbf{L}_1, \dots, \mathbf{L}_T$ from the data sequence. We first introduce a time-varying graph factor analysis (TGFA) to formulate the time-varying graph learning. By incorporating a graph evolution process into SGFA, we define TGFA as:

$$\mathbf{x}^{(t)} \sim \mathcal{N}(0, \mathbf{L}_t^\dagger + \sigma_\epsilon^2 \mathbf{I}), \quad (13)$$

$$\mathbf{L}_t = \begin{cases} \mathbf{0} & t = 0 \\ \mathbf{L}_{t-1} + \Delta \mathbf{L}_t & t \geq 1. \end{cases} \quad (14)$$

where $\mathbf{x}^{(t)}$, \mathbf{L}_t , and $\Delta \mathbf{L}_t$ are a signal, the graph Laplacian of the underlying graph and a temporal graph variation at a given time t , respectively. In Section III-A, we discuss (13), which indicates that time-varying graph learning requires the time-varying observations to be smooth on the learned graphs at the corresponding time slots. Besides the smoothness criterion, our approach allows us to incorporate prior knowledge about temporal graph variation and will lead to more robust graph learning. Thus, we generalize the time-varying graph learning problem as that of solving the following optimization:

$$\min_{\mathbf{L}_t \in \mathcal{L}} \sum_{t=1}^T \text{Tr}(\mathbf{X}_t^\top \mathbf{L}_t \mathbf{X}_t) + f(\mathbf{L}_t) + \eta \sum_{t=2}^T R(\Delta \mathbf{L}_t \circ \mathbf{H}), \quad (15)$$

where \mathcal{L} is the valid set of graph Laplacians and is given by

$$\mathcal{L} = \{ \mathbf{L} \in \mathbb{R}^{N \times N} \mid \mathbf{L} = \mathbf{L}^\top, L_{ij} \leq 0 \ (i \neq j), \\ L_{ii} = - \sum_{j \neq i} L_{ij} \}, \quad (16)$$

$\mathbf{H} = \mathbf{I} - \mathbf{1}\mathbf{1}^\top$, $R(\Delta \mathbf{L}_t \circ \mathbf{H})$ is a regularization term that characterizes the temporal change in graph edges, that is, the off-diagonal elements of the temporal graph variation $\Delta \mathbf{L}_t$. The first term in (15) corresponds to the smoothness term in the static case (12), and quantifies the smoothness of the signals on time-varying graphs. The function in the second term $f(\mathbf{L}_t)$ is a regularization to avoid obtaining trivial solutions. This function, of which examples will be given later, depends on assumptions made about the graph model. The parameter η controls the regularization strength.

We reformulate the problem (15) with a constraint (16) by using weighted adjacency matrices. As shown in the following, this leads to a tractable formulation because using weighted adjacency matrices allows us to simplify the condition for the valid set. A problem equivalent to that of (15) is then given by:

$$\min_{\mathbf{W}_t \in \mathcal{W}_m} \sum_{t=1}^T \frac{1}{2} \|\mathbf{W}_t \circ \mathbf{Z}_t\|_1 + f(\mathbf{W}_t) + \eta \sum_{t=2}^T R(\mathbf{W}_t - \mathbf{W}_{t-1}), \quad (17)$$

where the valid set of weighted adjacency matrices is defined by

$$\mathcal{W}_m = \{ \mathbf{W} \in \mathbb{R}_+^{N \times N} \mid \mathbf{W} = \mathbf{W}^\top, W_{ii} = 0 \}. \quad (18)$$

The first term of (17) is equivalent to $\text{Tr}(\mathbf{X}_t^\top \mathbf{L}_t \mathbf{X}_t)$, given that [17]:

$$\text{Tr}(\mathbf{X}_t^\top \mathbf{L}_t \mathbf{X}_t) = \frac{1}{2} \text{Tr}(\mathbf{W}_t \mathbf{Z}_t) = \frac{1}{2} \|\mathbf{W}_t \circ \mathbf{Z}_t\|_1, \quad (19)$$

where \mathbf{Z}_t is the pairwise distance matrix defined by

$$(\mathbf{Z}_t)_{ij} = \sum_{k=1}^K \|(\mathbf{x}_k^{(t)})_i - (\mathbf{x}_k^{(t)})_j\|^2. \quad (20)$$

In this paper, we solve the optimization problem in (17) to learn a time-varying graph. Throughout this paper, we set the regularization for the weighted adjacency matrix to be:

$$f(\mathbf{W}_t) = -\alpha \mathbf{1}^\top \log(\mathbf{W}_t \mathbf{1}) + \beta \|\mathbf{W}_t\|_F^2, \quad (21)$$

where α and β are the parameters. The first term in (21) forces the degree on each node to be positive without preventing edge weights from becoming zero. The second term controls the sparsity of the resulting graphs. Lower value leads to sparser graphs, and higher value leads to denser graphs. Next, we describe how to select the regularization for the graph temporal variation $R(\cdot)$ and solve the optimization problem.

IV. LEARNING TIME-VARYING GRAPH WITH TEMPORAL VARIATION REGULARIZATION

A. Regularization of Graph Temporal Variation

The choice of regularization for the graph temporal variation should be based on our *a priori* knowledge of temporal graph evolution. In this paper, we consider two types of graph evolutions, which appear in many important applications, and define associated regularization parameters in each case.

1) *Formulation with Fused Lasso*: In the first model, we assume that most edges and their weights are likely to remain unchanged over a short-term time horizon **(P1)**. Thus, we select a regularizer $R(\cdot) = \|\cdot\|_1$ in (17) and formulate the optimization problem as:

$$\min_{\mathbf{W}_t \in \mathcal{W}_m} \sum_{t=1}^T \frac{1}{2} \|\mathbf{W}_t \circ \mathbf{Z}_t\|_1 + f(\mathbf{W}_t) + \eta \sum_{t=2}^T \|\mathbf{W}_t - \mathbf{W}_{t-1}\|_1, \quad (22)$$

A penalty on ℓ_1 -norm of the difference between neighboring time windows leads to a *fused Lasso* problem [37], which encourages sparse differences, leading to local temporal constancy of weighted adjacency matrices, and thus, solution graphs that tend to satisfy the **(P1)** property.

In order to make the optimization problem tractable, we rewrite (22) and (21) in vector form, with \mathbf{W}_t and \mathbf{Z}_t replaced by $\mathbf{w}_t \in \mathbb{R}_+^{N(N-1)/2}$ and $\mathbf{z}_t \in \mathbb{R}_+^{N(N-1)/2}$ respectively. Only the upper-triangular parts of \mathbf{W}_t and \mathbf{Z}_t are considered given that the graph is undirected.

Let us define $\mathbf{w} = [\mathbf{w}_1^T \mathbf{w}_2^T \dots \mathbf{w}_T^T]^T$, $\mathbf{z} = [\mathbf{z}_1^T \mathbf{z}_2^T \dots \mathbf{z}_T^T]^T$, and $\mathbf{d} = [\mathbf{d}_1^T \mathbf{d}_2^T \dots \mathbf{d}_T^T]^T$ where $\mathbf{d}_t = \mathbf{W}_t \mathbf{1}$. We also introduce the linear operators \mathbf{S} and Φ that satisfy $\mathbf{S}\mathbf{w} = \mathbf{d}$ and $\Phi\mathbf{w} = \mathbf{w} - \hat{\mathbf{w}}$ respectively, where $\hat{\mathbf{w}} = [\mathbf{w}_1^T \mathbf{w}_1^T \mathbf{w}_2^T \dots \mathbf{w}_{T-1}^T]^T$.

Then, we can rewrite (22) and (21) as

$$\min_{\mathbf{w} \in \mathcal{W}_v} 2\mathbf{z}^T \mathbf{w} - \alpha \mathbf{1}^T \log(\mathbf{S}\mathbf{w}) + \beta \|\mathbf{w}\|_2^2 + \eta \|\Phi\mathbf{w}\|_1, \quad (23)$$

where

$$\mathcal{W}_v = \left\{ \mathbf{w} \in \mathbb{R}^{TN(N-1)/2} \mid w_i \geq 0 \ (i = 1, 2, \dots) \right\} \quad (24)$$

represents the nonnegativity constraint. By expressing (18) in vector form, the symmetric and diagonal constraints of (18) can be simplified.

2) *Formulation with Group Lasso*: The second model aims at learning graphs having the **(P2)** property. This is achieved by choosing $R(\cdot) = \|\cdot\|_2$ as the regularizer in (17), leading to a *group Lasso* [38] penalty as follows:

$$\min_{\mathbf{W}_t \in \mathcal{W}_m} \sum_{t=1}^T \frac{1}{2} \|\mathbf{W}_t \circ \mathbf{Z}_t\|_1 + f(\mathbf{W}_t) + \eta \sum_{t=2}^T \|\mathbf{W}_t - \mathbf{W}_{t-1}\|_2, \quad (25)$$

where only the last term differs from (22). Group Lasso penalizes the sum of the ℓ_2 -norm, leading to a $\ell_{2,1}$ -norm that encourages sparsity in each group. In this formulation, the temporal variation of the weighted adjacency matrices at a certain time slot is regarded as one group. Thus the group Lasso yields graphs whose edge weights can vary significantly at a few time slots while they remain almost constant at all the other time slots, thus satisfying the **(P2)** property.

In order to make the optimization problem tractable, we rewrite (25) in the same manner as in the previous model as:

$$\min_{\mathbf{w} \in \mathcal{W}_v} \mathbf{z}^T \mathbf{w} - \alpha \mathbf{1}^T \log(\mathbf{S}\mathbf{w}) + \beta \|\mathbf{w}\|_2^2 + \eta \sum_j \|\Phi\mathbf{w}\|_2, \quad (26)$$

where $[\Phi\mathbf{w}]_j = \mathbf{w}_j^T - \mathbf{w}_{j-1}^T$, $j = 2, \dots, T$.

B. Optimization

We solve (22) and (25) with a primal-dual splitting (PDS) method [31], which solves a problem in the form,

$$\min_{\mathbf{w}} f_1(\mathbf{w}) + f_2(\mathbf{w}) + f_3(\mathbf{M}\mathbf{w}), \quad (27)$$

where f_1 is a differentiable convex function with gradient ∇f_1 and Lipschitz constant ξ ; f_2 and f_3 are proper lower semi-continuous convex functions which are proximal; and \mathbf{M} is a linear operator.

Many algorithms to solve (27) have been proposed [31], [39], [40]. In this proposed method, we use a forward-backward-forward (FBF) approach [41], which makes it possible to compute the proximal operators of functions f_2 and f_3 in parallel.

1) *Fused Lasso*: By introducing the indicator function of \mathcal{W}_v in (24), we rewrite (23) as follows:

$$\min_{\mathbf{w}} \mathbf{z}^T \mathbf{w} - \alpha \mathbf{1}^T \log(\mathbf{S}\mathbf{w}) + \beta \|\mathbf{w}\|_2^2 + \eta \|\Phi\mathbf{w}\|_1 + \iota_{\mathcal{W}_v}(\mathbf{w}), \quad (28)$$

where the indicator function $\iota_{\mathcal{W}_v}$ is defined by

$$\iota_{\mathcal{W}_v}(\mathbf{w}) = \begin{cases} 0 & w_i \geq 0 \\ \infty & \text{otherwise.} \end{cases} \quad (29)$$

The objective function (28) further reduces to the applicable form of the PDS as follows:

$$\begin{aligned} f_1(\mathbf{w}) &= \beta \|\mathbf{w}\|_2^2 \text{ with } \xi = 2\beta, \\ f_2(\mathbf{w}) &= 2\mathbf{z}^T \mathbf{w} + \iota_{\mathcal{W}_v}(\mathbf{w}), \\ f_3(\mathbf{v}) &= -\alpha \mathbf{1}^T \log(\mathbf{v}_1) + \eta \|\mathbf{v}_2\|_1, \\ \mathbf{M} &= \begin{bmatrix} \mathbf{S} \\ \Phi \end{bmatrix}, \end{aligned} \quad (30)$$

where the dual variable is $\mathbf{v} := \mathbf{M}\mathbf{w} = [\mathbf{v}_1^T \mathbf{v}_2^T]^T$.

The proximal operator of f_2 is given by

$$(\text{prox}_{\gamma(\|\cdot\|_1 + \iota_{\mathcal{W}_v})}(\mathbf{x}))_i = \begin{cases} 0 & x_i \leq \gamma \\ x_i - \gamma & \text{otherwise.} \end{cases} \quad (31)$$

Because f_3 is separable across variables, the proximal operator can be computed separately for each term (see (6)). The proximal operator for the log barrier function [36] as the first term of f_3 is given by

$$(\text{prox}_{\gamma(-\mathbf{1}^T \log(\cdot))}(\mathbf{x}))_i = \frac{x_i + \sqrt{x_i^2 + 4\gamma}}{2}. \quad (32)$$

The proximal operator for the ℓ_1 -norm, i.e., the second term in f_3 , is well known to be the element-wise soft-thresholding operation [36]:

$$(\text{prox}_{\gamma\|\cdot\|_1}(\mathbf{x}))_i = \begin{cases} 0 & |x_i| \leq \gamma \\ \text{sgn}(x_i)(|x_i| - \gamma) & \text{otherwise.} \end{cases} \quad (33)$$

See Algorithm 1 for the complete algorithm.

2) *Group Lasso*: Similarly, the second objective function (26) can be reduced to the applicable form of the PDS by replacing f_3 with

$$f_3(\mathbf{v}) = -\alpha \mathbf{1}^\top \log(\mathbf{v}_1) + \eta \sum_j \|(\mathbf{v}_2)_j\|_2, \quad (34)$$

where $[\mathbf{v}_2]_j = [\Phi \mathbf{w}]_j$. The proximal operator of the group Lasso in f_3 is well known to be the blockwise soft-thresholding operation [36]:

$$\text{prox}_{\gamma \|\cdot\|_2}([\mathbf{x}]_j) = \begin{cases} \mathbf{0} & \|\mathbf{x}\|_2 \leq \gamma \\ (1 - \gamma/\|\mathbf{x}\|_2)([\mathbf{x}]_j) & \text{otherwise.} \end{cases} \quad (35)$$

Because the proximal operator of the functions f_2 and f_3 can be computed efficiently, the second model can also be solved with the PDS algorithm. See Algorithm 1.

The computational complexity for both of our learning problems is $\mathcal{O}(N^2)$ per iteration. Because the optimization problem in the proposed method is convex and lower-semicontinuous, convergence of the algorithms is guaranteed.

Algorithm 1 Proposed PDS Algorithm for solving (23) and (26)

Input: $\mathbf{w}^{(0)}, \mathbf{v}_1^{(0)}, \mathbf{v}_2^{(0)}$

Output: $\mathbf{w}^{(i)}$

```

while  $\|\mathbf{w}^{(i+1)} - \mathbf{w}^{(i)}\|/\|\mathbf{w}^{(i)}\| > \epsilon$  do
   $\mathbf{y}^{(i)} = \mathbf{w}^{(i)} - \gamma(2\beta \mathbf{w}^{(i)} + \mathbf{S}^\top \mathbf{v}_1^{(i)} + \Phi^\top \mathbf{v}_2^{(i)})$ 
   $\bar{\mathbf{y}}_1^{(i)} = \mathbf{v}_1^{(i)} + \gamma(\mathbf{S} \mathbf{w}^{(i)})$ 
   $\bar{\mathbf{y}}_2^{(i)} = \mathbf{v}_2^{(i)} + \gamma(\Phi \mathbf{w}^{(i)})$ 
   $\mathbf{p}^{(i)} = \text{prox}_{\gamma(\|\cdot\|_1 + \iota_{\mathcal{W}_v})}(\mathbf{y}^{(i)})$ 
   $\bar{\mathbf{p}}_1^{(i)} = \bar{\mathbf{y}}_1^{(i)} - \gamma \text{prox}_{\frac{1}{\gamma}(-\mathbf{1}^\top \log(\cdot))}(\frac{\bar{\mathbf{y}}_1^{(i)}}{\gamma})$ 
   $\bar{\mathbf{p}}_2^{(i)} = \begin{cases} \bar{\mathbf{y}}_2^{(i)} - \gamma \text{prox}_{\frac{1}{\gamma}\|\cdot\|_1}(\frac{\bar{\mathbf{y}}_2^{(i)}}{\gamma}) & \text{for solving (23)} \\ \bar{\mathbf{y}}_2^{(i)} - \gamma \text{prox}_{\frac{1}{\gamma}\|\cdot\|_2}(\frac{\bar{\mathbf{y}}_2^{(i)}}{\gamma}) & \text{for solving (26)} \end{cases}$ 
   $\mathbf{q}^{(i)} = \mathbf{p}^{(i)} - \gamma(2\beta \mathbf{p}^{(i)} + \mathbf{S}^\top \bar{\mathbf{p}}_1^{(i)} + \Phi^\top \bar{\mathbf{p}}_2^{(i)})$ 
   $\bar{\mathbf{q}}_1^{(i)} = \bar{\mathbf{p}}_1^{(i)} + \gamma(\mathbf{S} \mathbf{p}^{(i)})$ 
   $\bar{\mathbf{q}}_2^{(i)} = \bar{\mathbf{p}}_2^{(i)} + \gamma(\Phi \mathbf{p}^{(i)})$ 
   $\mathbf{w}^{(i+1)} = \mathbf{w}^{(i)} - \mathbf{y}^{(i)} + \mathbf{q}^{(i)}$ 
   $\mathbf{v}_1^{(i+1)} = \mathbf{v}_1^{(i)} - \bar{\mathbf{y}}_1^{(i)} + \bar{\mathbf{q}}_1^{(i)}$ 
   $\mathbf{v}_2^{(i+1)} = \mathbf{v}_2^{(i)} - \bar{\mathbf{y}}_2^{(i)} + \bar{\mathbf{q}}_2^{(i)}$ 
end while

```

V. EXPERIMENTAL RESULTS WITH SYNTHETIC DATASET

In this section, we present the experimental results with synthetic data and compare the performance of our proposed method with related graph learning methods (see Table II for a summary of all the methods we compare).

A. Synthetic Datasets

We create three types of synthetic graph signals generated from time-varying graphs: A time-varying graph based on random waypoint model (abbreviated as TV-RW graph) [42], a time-varying Erdős-Rényi graph (TV-ER graph), and the ER graph that gives large fluctuations at a few time slots (LF-ER graph).

The dataset construction consists of two steps:

- 1) Constructing a time-varying graph.
- 2) Generating time-varying graph signals from probability distributions based on graph Laplacians of the created time-varying graph.

We then describe the details of three datasets by referring to the desired properties **(P1)** and **(P2)** described in Section I.

1) *Time-Varying Graph Construction*: The TV-RW graph is constructed in two steps. First, we simulate the RW model to obtain the time-varying coordinates over time. The model simulates some sensors moving around a square space of 400 m² with random speed and directions. We obtain the time varying data corresponding to the position of each sensor at any given time. The number of sensors is set to $N = 36$ and the motion speeds is set in the range of 0.05–0.5 m/s. We sample sensor positions every 0.1 s for a total of 300 observations. In the second step, we construct a 3-nearest-neighbor graph at each time from the position data. These edge weights are given by

$$w(i, j) = \exp\left(-\frac{\text{dist}(i, j)}{2\theta}\right), \quad (36)$$

where $\text{dist}(i, j)$ is the Euclidean distance between nodes i and j , and θ is a parameter. The edge weights in this graph generally vary smoothly as in (36); however, some edges will (dis)appear in the next time slot due to the nature of the k -neighborhood graph. Note that our method estimates time-varying graphs robustly for various k . This graph partially satisfies **(P1)** because the topology mostly remains unchanged in a short time horizon while the edge weights change smoothly over time.

The TV-ER graph is constructed by varying edges in an ER graph over time. We first construct an initial static ER graph \mathbf{W}_1 with $N = 36$ and an edge connection probability $p = 0.05$. The obtained graph satisfies **(P1)**. The t th graph \mathbf{W}_t is obtained by resampling 5% of edges from the previous graph \mathbf{W}_{t-1} . In this way, we construct a set of graphs that varies over 300 time slots. The edge weights on this graph are set to be uniformly distributed in the interval $[0, 1]$. Once they are randomly selected, they remain fixed until the edges are resampled. In this graph, only a few edges switch at any given time while most of the edges remain unchanged, i.e., this graph also follows **(P1)**.

The LF-ER graph is a simulated example of the time-varying graph with **(P2)**. It is often observed in temporal brain connectivity dynamics [43], [44]. First, we generate six connectivity states, i.e., six static graphs. Each of the graph is an ER graph with $N = 36$ and an edge connection probability $p = 0.05$.¹ Second, the initial state is selected randomly from the six states. Its state remains unchanged with a 98% probability and changes to another connectivity state with the 2% probability at each time. This graph follows the **(P2)** property. An LF-ER is constructed in this way and we have 300 observations in time.

¹In our preliminary experiments, p hardly affects the graph learning performances.

TABLE II
LIST OF ALTERNATIVE AND PROPOSED METHODS

	Method	Approach	Temporal Regularization
Static	SGL-Glasso [19] SGL-Smooth [17]	Graphical Lasso based model Signal smoothness model	- -
Time-Varying	TGL-Tikhonov [33] TGL-FLasso (proposed) TGL-GLTV (proposed)	Signal smoothness + Regularization Signal smoothness + Regularization Signal smoothness + Regularization	Tikhonov regularization Fused Lasso Group Lasso

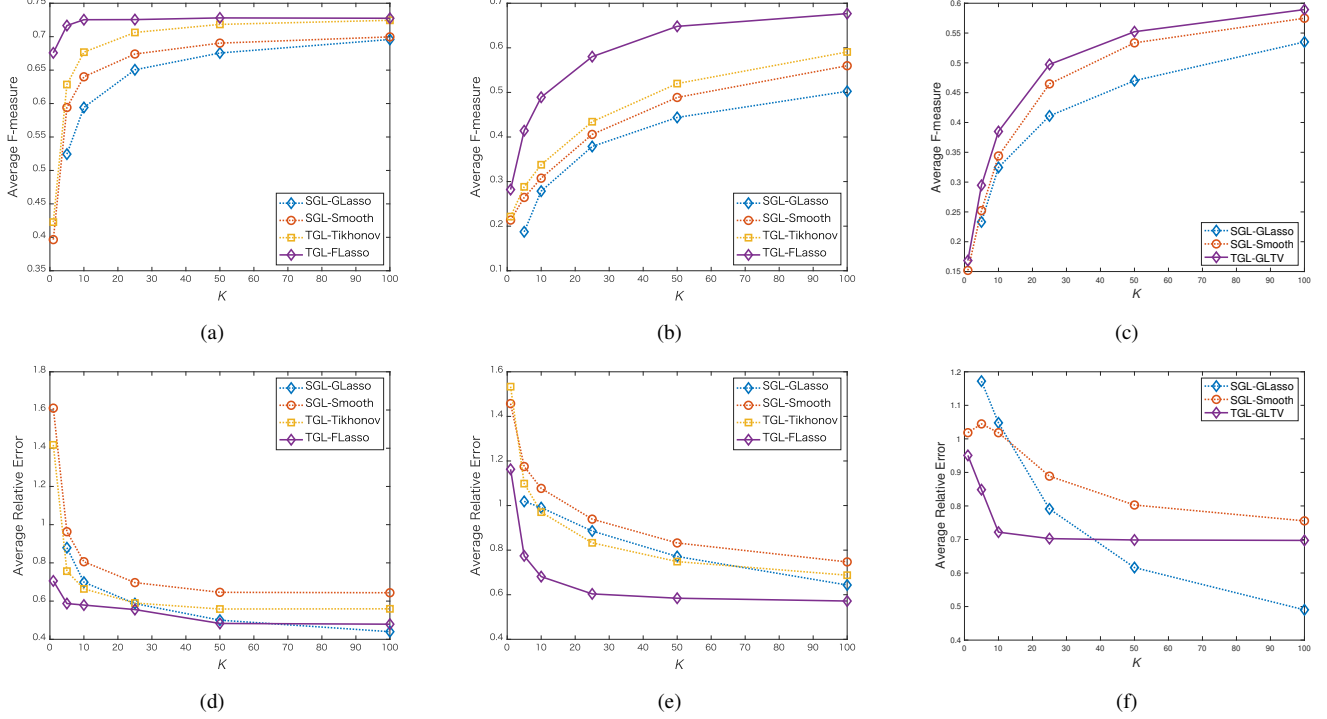


Fig. 2. The performance of learning time-varying graph for different number of data samples. Top row demonstrates the F-measure for the datasets based on TV-RW graph, TV-ER graph, and the graph that occurs large fluctuations at a few time slots, respectively. Bottom row demonstrates the relative error for those datasets.

2) *Generating Data Samples*: We create data samples from the constructed time-varying graphs in the same manner for all the graphs. Let \mathbf{L}_t be the graph Laplacian corresponding to \mathbf{W}_t . A data sample \mathbf{x}_t is generated from a Gaussian Markov random field model defined by

$$p(\mathbf{x}_t | \mathbf{L}^{(t)}) = \mathcal{N}(\mathbf{x}_t | 0, (\mathbf{L}_t + \sigma^2 \mathbf{I})^{-1}), \quad (37)$$

where σ^2 is the covariance of the Gaussian noise. We set $\sigma = 0.5$ in this experiments. Pairs of variables generated from this distribution have closer values to each other when the corresponding nodes connect with a larger edge weight.

B. Performance Comparison

1) *Experimental Conditions*: We evaluate the performance in terms of relative error and F-measure, each averaged over all the time slots. Relative error is given by

$$\text{Relative error} = \frac{\|\widehat{\mathbf{W}} - \mathbf{W}^*\|_F}{\|\mathbf{W}^*\|_F}, \quad (38)$$

where $\widehat{\mathbf{W}}$ is the estimated weighted adjacency matrix, and \mathbf{W}^* is the ground truth. It reflects the accuracy of edge weights on the estimated graph. The F-measure is given by

$$\text{F-measure} = \frac{2\text{tp}}{2\text{tp} + \text{fn} + \text{fp}}, \quad (39)$$

where the true positive (tp) is the number of edges that are included both in $\widehat{\mathbf{W}}$ and \mathbf{W}^* , the false positive (fn) is the number of edges that are not included in $\widehat{\mathbf{W}}$ but are included in \mathbf{W}^* , and the false negative (fp) is the number of edges that are included in $\widehat{\mathbf{W}}$ but are not included in \mathbf{W}^* . The F-measure, which is the harmonic average of the precision and recall, represents the accuracy of the estimated graph topology. The F-measure takes values between 0 and 1. The higher the F-measure is, the higher the performance of capturing graph topology is.

In this experiment, our goal is to compare all the methods based on their best achievable performance. We perform Monte-Carlo simulations for each method to find the parameters minimizing relative error. Note that as shown in the next section, fixed parameters still work well for our graph learning with real dataset. For SGL-Smooth, TGL-Tikhonov,

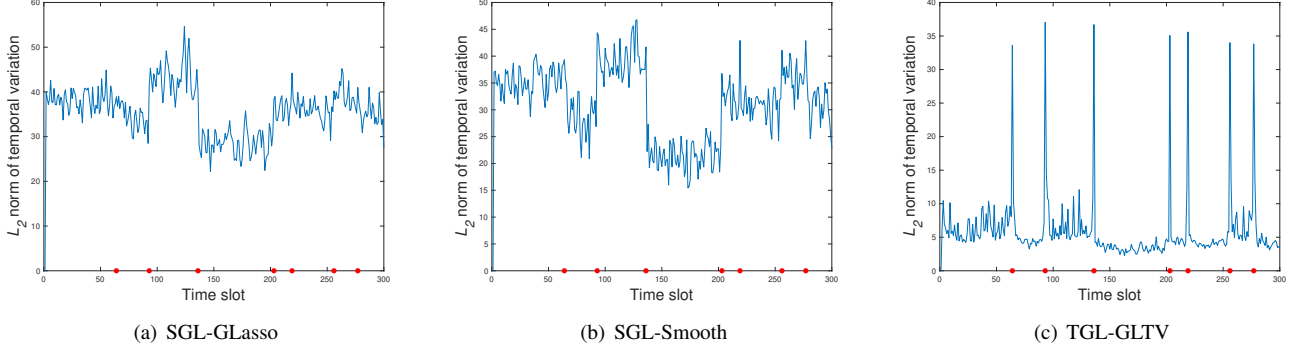


Fig. 3. The visualization of the temporal variations in the time-varying graph learned from the dataset based on the graph in which large fluctuations occur at a few time slots. Red points in these figures represent time slots where the connectivity state changes.

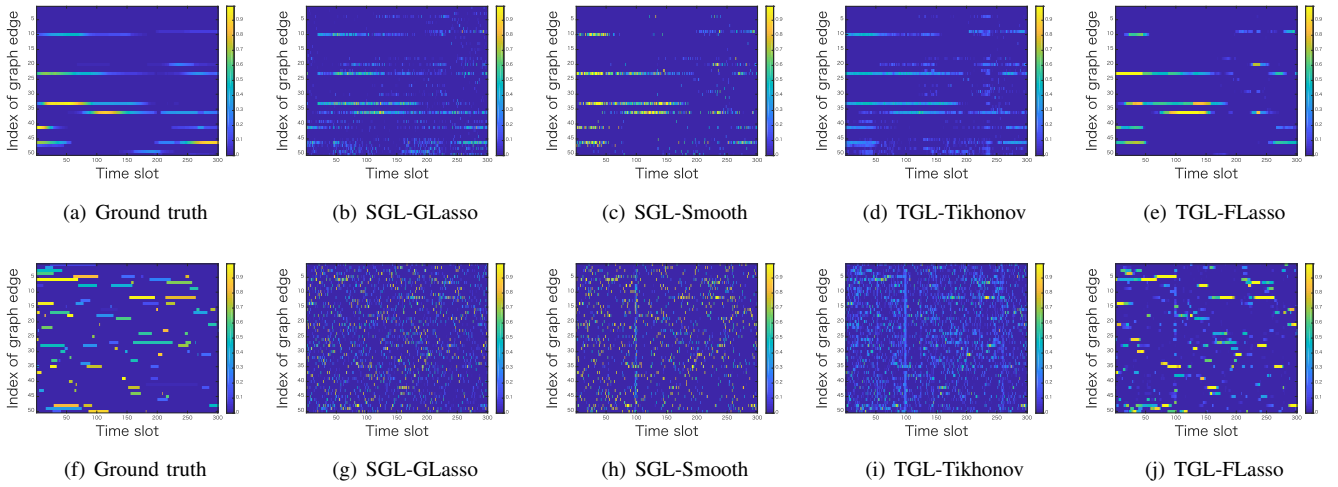


Fig. 4. The visualization of the temporal variations in the time-varying graph. Top row demonstrates the variations for the dataset based on the TV-RW graph. Bottom row is the variations for TV-ER graph datasets. Colors in these figures represent the weights of the edges.

TGL-FLasso, and TGL-GLTV, α is selected by fine-tuning, and β is selected from the following set:

$$\{0\} \cup \{0.75^r z_{\max} \mid r = 1, 2, \dots, 14\}, \quad (40)$$

where $z_{\max} = \max_{i \neq j}(\mathbf{Z})_{ij}$. The parameter η for TGL-FLasso and TGL-GLTV is selected from 0.1 to 2 in steps of 0.1. The parameter for SGL-GLasso is selected by the method described in [19]. The tolerance value ϵ in Algorithm 1 is set to 1.0×10^{-3} . We evaluate the performance for each method with the different number of data samples $K = \{1, 5, 10, 25, 50, 100\}$ and measure the average of the relative error and the F-measure over all the time frames. Note that SGL-GLasso is not evaluated with $K = 1$ because the sample covariance used in SGL-GLasso cannot be calculated.

2) *Results*: Fig. 2 shows the performance comparisons according to K . Figs. 2(a) and (d) show the average F-measure and the relative error for TV-RW graphs; Figs. 2(b) and (e) show those for TV-ER graphs; Figs. 2(c) and (f) show those for LF-ER graphs.

As shown in Fig. 2, the existing static graph learning methods, i.e., SGL-GLasso and SGL-Smooth, present worse performance than the time-varying methods. This is because SGL-Smooth learns a graph from each time slot independently.

It does not consider the temporal relation of graphs. Note that SGL-GLasso sometimes presented a comparable performance with time-varying methods when K is large.

Fig. 2(a) and (d) present that TGL-FLasso outperforms TGL-Tikhonov despite the fact that the edges in a TV-RW graph vary smoothly in this case. This would be because TGL-Smooth yields undesirable edges (discussed later in this section). The TGL-FLasso significantly outperforms the other methods for TV-ER graphs as shown in Figs. 2(b) and (d). This indicates that the fused Lasso constraint on the difference between graphs in neighboring time slots works well.

It is also worth noting that, thanks to the regularization term, TGL-FLasso can successfully learn accurate time-varying graphs from a smaller number of measurements. As can be seen in Fig. 2, the performance gain for TV-ER graphs is much better than that of TV-RW graphs. This is because the TV-ER graphs have the **(P1)** property while the TV-RW graphs lack a part of **(P1)**, as previously mentioned.

Focusing on Fig. 2(c) and (f), TGL-GLTV also outperforms the static graph learning methods for small K . Fig. 3 shows the L_2 -norm of the temporal difference of learned adjacency matrices in each time slots, i.e., $\|\mathbf{W}_t - \mathbf{W}_{t-1}\|_2$. Clearly, it

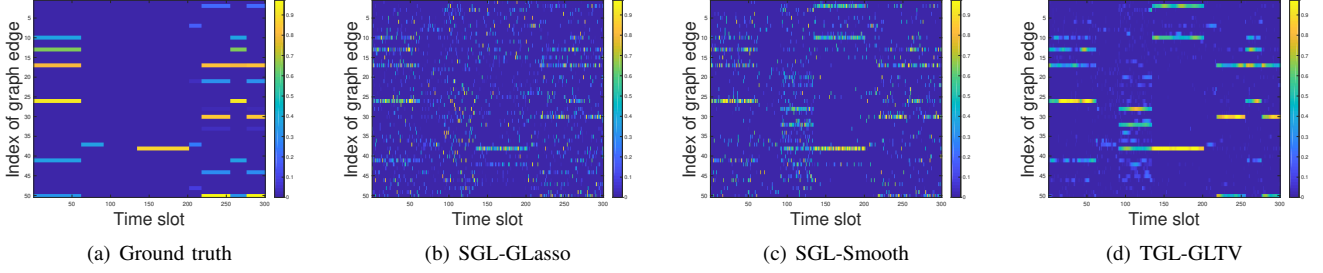


Fig. 5. The visualization of the temporal variations in the time-varying graph learned from the dataset based on the graph that produces large fluctuations at few time slots.

can be observed that TGL-GLTV can detect large fluctuations of the graph in time slots where the connectivity state changes, while SGL-GLasso and SGL-Smooth have several unclear jumps. As a result, TGL-GLTV is the graph learning method suitable for change detection, and the group Lasso of temporal variation is effective in graph learning.

Fig. 4 visualizes the temporal variation of a part of edge weights on the learned graphs from the datasets of TV-RW and TV-ER graphs with $K = 10$. The vertical and horizontal axis of these figures represent the edge and time slot indices of the learned graph, and the color represents the intensity of the edge weights. To make an easy view, they visualize the first 50 edge indices. As can be seen in Fig. 4, SGL-GLasso and SGL-Smooth cannot capture the original graph structure, and they output the graphs ignoring its temporal relations. TGL-Tikhonov is slightly superior to the static graph learning methods. However, it yields many undesirable edges and the edge weights are relatively small. In contrast, TGL-FLasso estimated the original structure better than the other methods and outputs the graph considering its temporal relationships.

Fig. 5 also demonstrates the temporal variation for the datasets of the LF-ER graph with $K = 10$. It can be observed that SGL-GLasso and SGL-Smooth cannot capture the large fluctuations in the graph. In contrast, TGL-GLTV detects large edge changes in the original time-varying graph.

C. Effect of Temporal Resolution

To verify the robustness of the proposed method against the temporal graph transition, i.e., temporal resolution, we evaluate the performance for the dataset of the TV-RW graph with different sampling periods $\tau = 0.1, 0.5, 1.0, 1.5, 2.0$. Table III shows the performance comparisons with the dataset of TV-RW graph with $K = 10$ according to τ . TGL-FLasso outperforms other methods when the sampling period τ is small. On the other hand, TGL-FLasso and TGL-Tikhonov have comparable performance for the average relative error with $\tau = 1.0$, and TGL-FLasso gets worse performance than TGL-Tikhonov when τ gets large. This is because many edge weights of graphs may vary over time when the sampling period is long, i.e., it does not satisfy (P1).

D. Computation Time

We compare the computation time of the proposed methods with some related works. All methods are implemented in

TABLE III
THE PERFORMANCE OF LEARNING TIME-VARYING GRAPH FOR DIFFERENT SAMPLING PERIODS.

Average F-measure					
Sampling period	0.1	0.5	1.0	1.5	2.0
SGL-GLasso	0.613	0.574	0.574	0.580	0.575
SGL-Smooth	0.639	0.562	0.562	0.563	0.534
TGL-Tikhonov	0.681	0.606	0.613	0.611	0.596
TGL-FLasso	0.718	0.636	0.656	0.664	0.627
Average Relative Error					
Sampling period	0.1	0.5	1.0	1.5	2.0
SGL-GLasso	0.602	0.690	0.699	0.697	0.696
SGL-Smooth	0.612	0.683	0.692	0.685	0.731
TGL-Tikhonov	0.529	0.606	0.607	0.605	0.633
TGL-FLasso	0.431	0.574	0.609	0.656	0.701

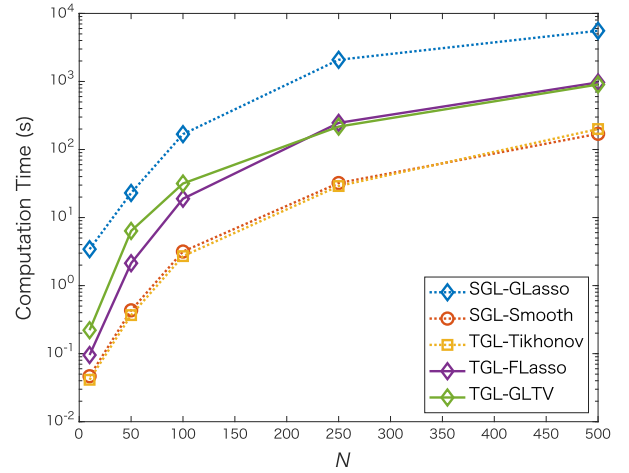


Fig. 6. The comparison of computation time for the different number of N .

MATLAB R2018b and run on a 2.3-GHz Intel Xeon W processor with 128-GB RAM. The experiments are tested on the TV-ER graph dataset for different number of nodes $N = \{10, 50, 100, 250, 500\}$. The tolerance value ϵ in each methods is set to 1.0×10^{-3} .

Fig. 6 shows the computation time of each method, demonstrating that the proposed methods (TGL-FLasso and TGL-GLTV) converge faster than SGL-GLasso. Because SGL-GLasso needs to solve nonnegative quadratic programs as the subproblem in each iteration, it requires very significant computation time. The computational complexity of

TABLE IV
DENOISING RESULTS

	<i>dog</i>	<i>handstand</i>	<i>skirt</i>	<i>wheel</i>
noisy	12.12	13.97	13.73	15.45
k -NN	12.35	14.29	14.01	15.76
SGL-Smooth	13.13	15.37	15.03	16.74
TGL-Tikhonov	13.34	15.69	15.34	17.06
TGL-FLasso	20.05	21.32	21.58	22.97

one iteration in SGL-GLasso is $\mathcal{O}(N^2 + T_p(N))$ complexity where $\mathcal{O}(T_p(N))$ is the worst-case complexity of solving the subproblem, and $T_p(N) = \Omega(N^3)$. On the other hand, the complexity the iteration in TGL-FLasso and TGL-GLTV is $\mathcal{O}(N^2)$ complexity as described in Section IV.

TGL-FLasso and TGL-GLTV required longer computation time than SGL-Smooth and TGL-Tikhonov, where they estimate a graph using the almost same algorithm; that is, they have the same computational complexity $\mathcal{O}(N^2)$. However, TGL-FLasso and TGL-GLTV introduce dual variables to solve the optimization problem with temporal variation regularization, i.e., they have more variables to update than SGL-Smooth and TGL-Tikhonov. Although TGL-Tikhonov also has temporal variation regularization, it can be computed without introducing dual variable because its temporal variation regularization can be differentiable.

VI. REAL DATA APPLICATIONS

A. Denoising of Dynamic Point Clouds

Our proposed method is applied to dynamic point cloud data denoising. Dynamic point cloud data contains 3D coordinates of dynamically evolving points. When point cloud data are acquired, the measurement error leads to the displacements of the geometric coordinates of the point clouds. Here, we consider graph-based denoising approaches. The performance of noise removal depends on the underlying graph. In this experiment, denoising is performed by using graph heat kernel filtering [45]. The time-varying graph used in the denoising is estimated from noisy point cloud data.

We use the dynamic point cloud dataset in [46], which contains five dynamic point clouds: *dance*, *dog*, *handstand*, *skirt*, and *wheel*. As this dataset is clean data, with position ranges from -260 to 1932 , we added Gaussian noise with $\sigma = 90$, which is a significantly higher noise level. The time-varying graph is learned from the dataset downsampled to 357 points and evolving over 240 time slots. In this experiment, we use fixed parameters for each method, which is determined by a grid search with *dance* data, and evaluate the denoising performance with the other four data.

Table IV summarizes the dynamic point cloud denoising qualities. Time-varying graph learning methods, TGL-Tikhonov and TGL-FLasso, show better results than SGL-Smooth and k -nearest neighbor. This indicates that the k -nearest neighbor cannot construct the meaningful graph from noisy data. Additionally, TGL-FLasso outperformed TGL-Tikhonov up to 6 dB.

Fig. 7 shows the visualization of denoising results of the *wheel* at a certain time. Similar to the numerical performance,

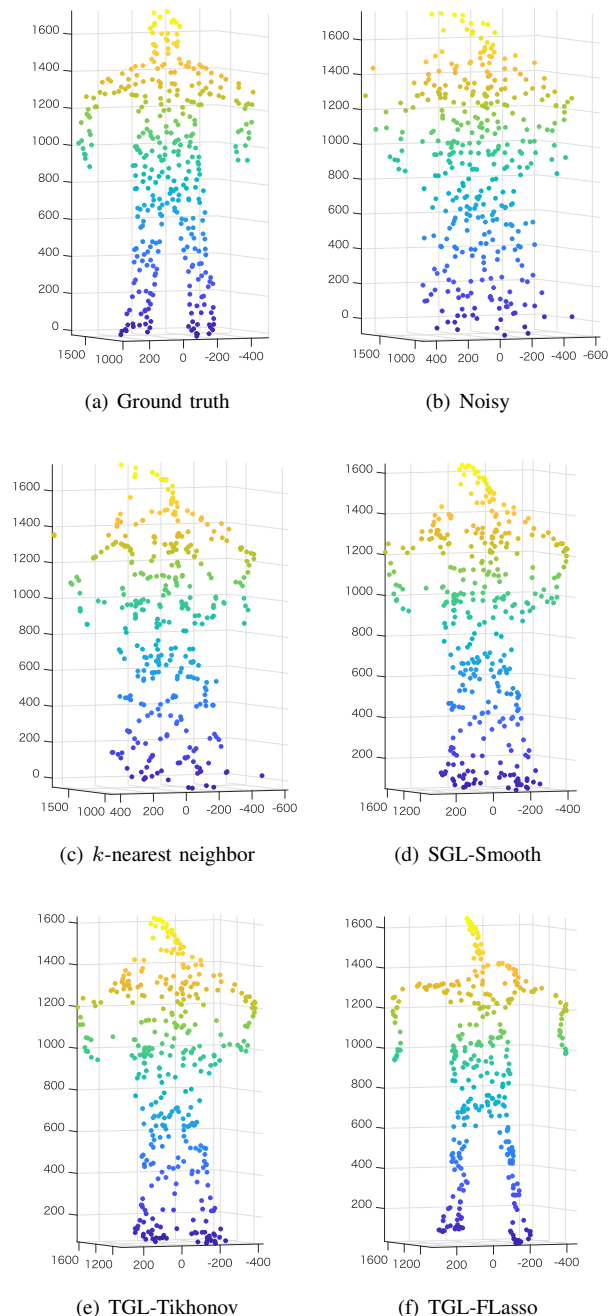


Fig. 7. The visualization of denoising result of *wheel* at a certain time.

the k -nearest neighbor cannot capture the structure of the human body. SGL-Smooth and TGL-Tikhonov yield slightly better outputs than that by the k -nearest neighbor; however, the arms and legs are still problematic. On the other hand, TGL-FLasso can successfully capture the structure of the human body than the other methods.

Fig. 8 visualizes a graph at a certain time in the time-varying graph estimated from the noisy *wheel* data in the dynamic point cloud dataset. In this figure, the nodes in the graphs are plotted in the correct position for visualization. As shown in Fig. 8, k -nearest neighbor yields a sparse graph but nodes are connected without a temporal relationship. SGL-

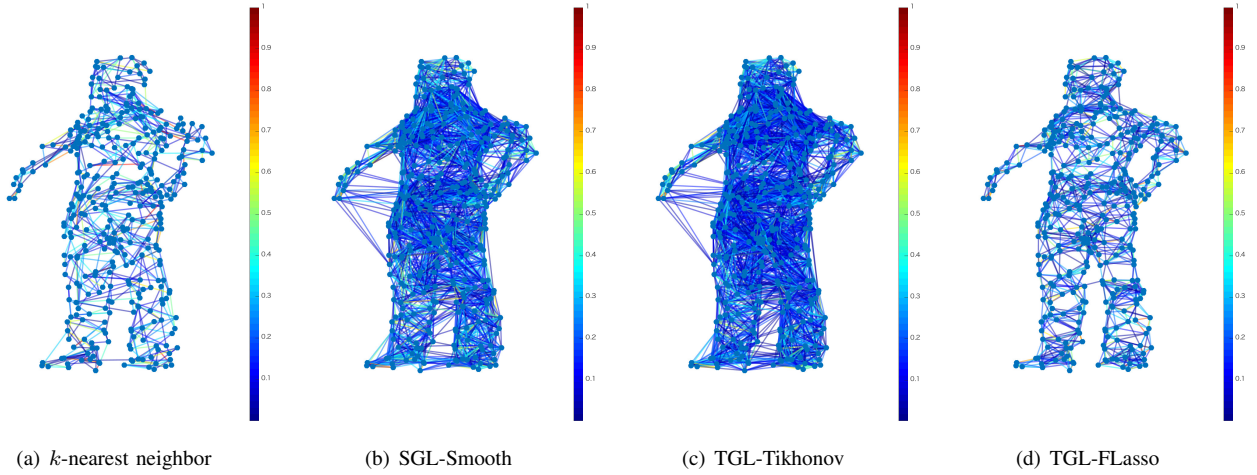


Fig. 8. The visualization of a graph at a certain time in the time-varying graph learned from the noisy point cloud data.

Smooth and TGL-Tikhonov yielded very dense edges along with connecting different parts in the body. In contrast, TGL-FLasso yields the graph whose nodes are connected accurately and preserves the human body structure.

B. Application to Temperature Data

Finally, we apply the proposed method to estimate a time-varying graph from temperature data in the island of Hokkaido, the northernmost region in Japan. The goal of this experiment is to learn a time-varying graph to explore the relationship between geographical regions over time. In this experiment, we use the average daily temperature data² collected from 172 locations in Hokkaido in 2015, i.e., overall the dataset has 365 time slots with $N = 172$ and $K = 24$. From this data, we estimate a time-varying graph by using TGL-FLasso.

Fig. 9 shows the graph learned from temperature data³. From the figure, the inferred characteristics of the learned graph are as follows:

- Nodes close to each other are basically connected. This is reasonable because the temperature is similar in the same geographical area. Note that, if the recording points are separated by mountain ranges, nodes may not be connected even if the distances are short.
- Nodes along the coast are often connected to each other, and the inland nodes are also connected to each other. Especially, coastal nodes may connect to each other despite being far away.
- Locally connected structures in the learned graph mostly remain unchanged over time as shown in Fig. 9(d).

Figs. 9(e) and 9(f) show the season-specific graphs. We have found that a coastal node often has a connection to another coastal node even if they are not close to each other. This can be justified by the warming or cooling effect of sea currents that occur seasonally in this area and that affect coastal areas in similar ways. Fig. 10 represents daily sea surface temperatures

(SST) on January 8 and August 9, 2015⁴. As can be seen in Figs. 9(e), 9(f), and 10, nodes in similar SST areas are connected to each other in the learned graph. It is important to emphasize that there was no prior information about the SST areas used in the graph learning process.

VII. CONCLUSION

In this paper, we have presented a framework for learning time-varying graphs suitable for analysis of spatiotemporal data and change detection. The framework formulates a time-varying graph learning problem as convex optimization problems with the constraints on the temporal variation in the graph. Specifically, the framework introduces fused Lasso regularization and group Lasso regularization of the temporal variation to learn the graph having temporal homogeneity and one reflecting sudden change in networks respectively. We also propose algorithms solving the optimization problems based on the primal-dual splitting algorithm. In the applications on the synthetic and real data, we demonstrated that our proposed model can successfully learn the time-varying graphs, especially under the condition that the number of observations is small. Our future work includes implementing an automatic parameter tuning method and extending the algorithm for online graph learning.

REFERENCES

- [1] C. Nowzari, V. M. Preciado, and G. J. Pappas, "Analysis and control of epidemics: A survey of spreading processes on complex networks," *IEEE Control Syst. Mag.*, vol. 36, no. 1, pp. 26–46, 2016.
- [2] A. Ganesh, L. Massoulie, and D. Towsley, "The effect of network topology on the spread of epidemics," in *Proceedings IEEE 24th Annual Joint Conference of the IEEE Computer and Communications Societies.*, vol. 2, 2005, pp. 1455–1466 vol. 2.
- [3] V. Colizza, A. Barrat, M. Barthélemy, and A. Vespignani, "The role of the airline transportation network in the prediction and predictability of global epidemics," *PNAS*, vol. 103, no. 7, pp. 2015–2020, 2006.
- [4] J. Zhang and J. M. F. Moura, "Diffusion in social networks as SIS epidemics: Beyond full mixing and complete graphs," *IEEE J. Sel. Top. Signal Process.*, vol. 8, no. 4, pp. 537–551, 2014.

²The Japan Meteorological Agency provided the daily temperature data from their website at <https://www.jma.go.jp/jma/index.html>

³The Geospatial Information Authority of Japan provided the map in Hokkaido with altitude from their website at <http://www.gsi.go.jp/>

⁴The daily SST was provided by Japan Meteorological Agency, from their website at <https://www.jma.go.jp/jma/index.html>

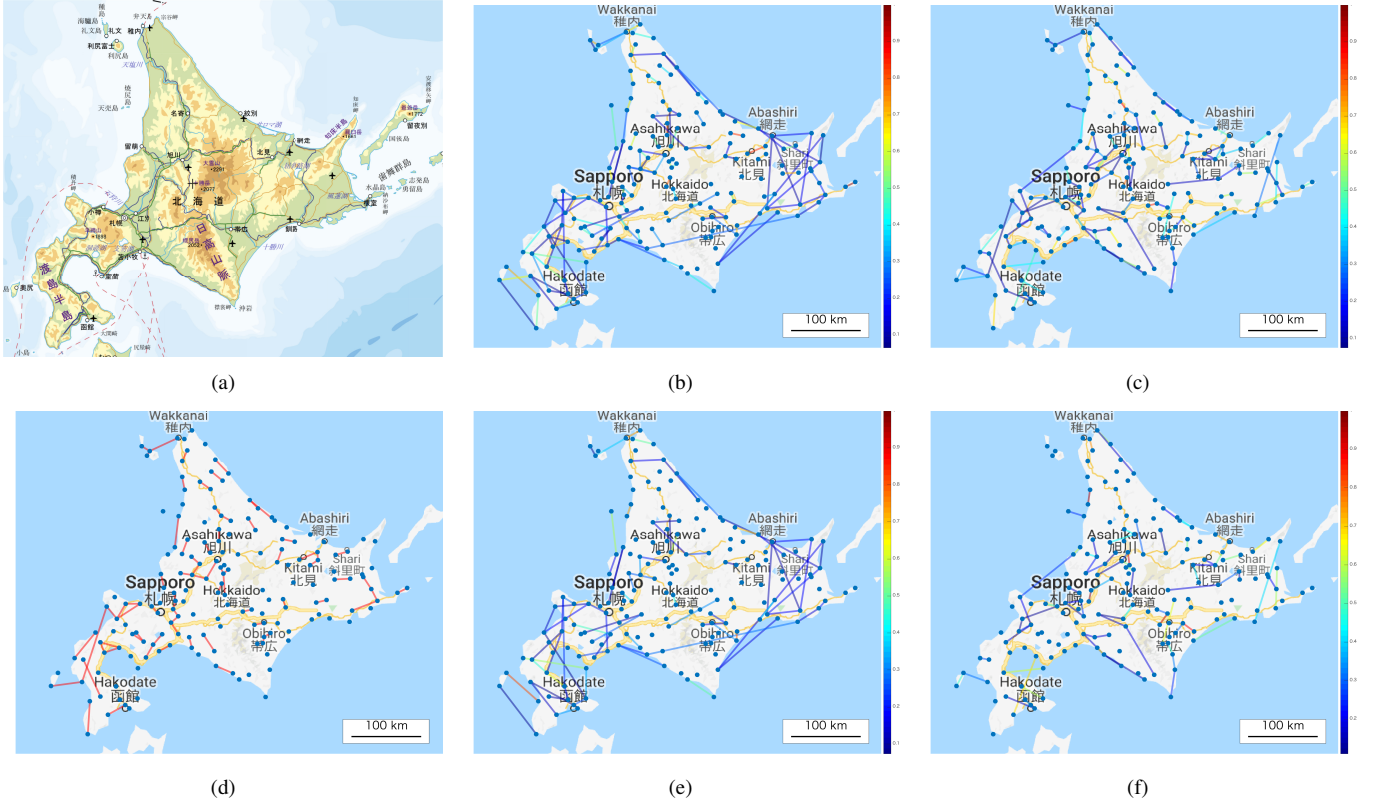


Fig. 9. The visualization of the graph learned from the temperature data. (a) Map of Hokkaido with altitude. (b) The graph learned on January 8, 2015 (winter graph). (c) The graph learned on August 9, 2015 (summer graph). (d) Edges common in winter and summer. (e) The winter graph from which the common edges have been removed (winter-specific graph). (f) The summer graph from which the common edges have been removed (summer-specific graph).

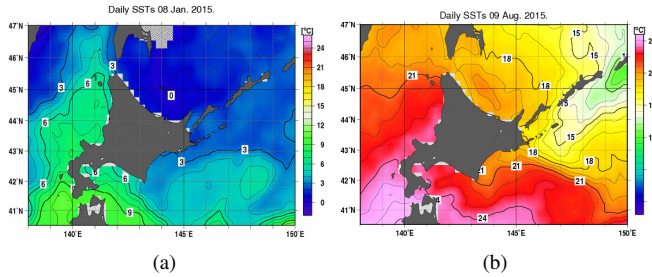


Fig. 10. Daily sea surface temperature (SST) on (a) 8 January 2015. (b) 9 August 2015.

[5] N. Shahid, N. Perraudin, V. Kalofolias, G. Puy, and P. Vandergheynst, “Fast robust PCA on graphs,” *IEEE J. Sel. Top. Signal Process.*, vol. 10, no. 4, pp. 740–756, 2016.

[6] F. Shang, L. C. Jiao, and F. Wang, “Graph dual regularization non-negative matrix factorization for co-clustering,” *Pattern Recognition*, vol. 45, no. 6, pp. 2237–2250, 2012.

[7] Z. Zhang and K. Zhao, “Low-rank matrix approximation with manifold regularization,” *IEEE Trans. Pattern Anal. Mach. Intell.*, vol. 35, no. 7, pp. 1717–1729, 2013.

[8] A. Gadde, S. K. Narang, and A. Ortega, “Bilateral filter: Graph spectral interpretation and extensions,” in *Proc. IEEE Int. Conf. Image Process.*, 2013, pp. 1222–1226.

[9] Y. Wang, A. Ortega, D. Tian, and A. Vetro, “A graph-based joint bilateral approach for depth enhancement,” in *Proc. IEEE Int. Conf. Acoust. Speech. Signal Process.*, 2014, pp. 885–889.

[10] M. Onuki, S. Ono, M. Yamagishi, and Y. Tanaka, “Graph signal denoising via trilateral filter on graph spectral domain,” *IEEE Trans. Signal Inf. Process. Netw.*, vol. 2, no. 2, pp. 137–148, 2016.

[11] A. Elmoataz, O. Lezoray, and S. Bougleux, “Nonlocal discrete regu-

larization on weighted graphs: A framework for image and manifold processing,” *IEEE Trans. Image Process.*, vol. 17, no. 7, pp. 1047–1060, 2008.

[12] C. Couprie, L. Grady, L. Najman, J. Pesquet, and H. Talbot, “Dual constrained TV-based regularization on graphs,” *SIAM J. Imaging Sci.*, vol. 6, no. 3, pp. 1246–1273, 2013.

[13] S. Ono, I. Yamada, and I. Kumazawa, “Total generalized variation for graph signals,” in *Proc. IEEE Int. Conf. Acoust. Speech. Signal Process.*, 2015, pp. 5456–5460.

[14] X. Dong, D. Thanou, M. Rabbat, and P. Frossard, “Learning graphs from data: A signal representation perspective,” *IEEE Signal Process. Mag.*, vol. 36, no. 3, pp. 44–63, 2019.

[15] G. Mateos, S. Segarra, A. G. Marques, and A. Ribeiro, “Connecting the dots: Identifying network structure via graph signal processing,” *IEEE Signal Process. Mag.*, vol. 36, no. 3, pp. 16–43, 2019.

[16] G. B. Giannakis, Y. Shen, and G. V. Karanikolas, “Topology identification and learning over graphs: Accounting for nonlinearities and dynamics,” *Proc. IEEE*, vol. 106, no. 5, pp. 787–807, 2018.

[17] V. Kalofolias, “How to learn a graph from smooth signals,” in *Proc. Int. Conf. Artif. Intell. Statist.*, 2016, pp. 920–929.

[18] X. Dong, D. Thanou, P. Frossard, and P. Vandergheynst, “Learning Laplacian matrix in smooth graph signal representations,” *IEEE Trans. Signal Process.*, vol. 64, no. 23, pp. 6160–6173, 2016.

[19] H. E. Egilmez, E. Pavez, and A. Ortega, “Graph learning from data under Laplacian and structural constraints,” *IEEE J. Sel. Top. Signal Process.*, vol. 11, no. 6, pp. 825–841, 2017.

[20] B. Pasdeloup, V. Gripon, G. Mercier, D. Pastor, and M. G. Rabbat, “Characterization and inference of graph diffusion processes from observations of stationary signals,” *IEEE Trans. Signal Inf. Process. Netw.*, vol. 4, no. 3, pp. 481–496, 2018.

[21] D. Thanou, X. Dong, D. Kressner, and P. Frossard, “Learning heat diffusion graphs,” *IEEE Trans. Signal Inf. Process. Netw.*, vol. 3, no. 3, pp. 484–499, 2017.

[22] J. Mei and J. M. F. Moura, “Signal processing on graphs: Causal modeling of unstructured data,” *IEEE Trans. Signal Process.*, vol. 65, no. 8, pp. 2077–2092, 2017.

- [23] S. P. Chepuri, S. Liu, G. Leus, and A. O. Hero, "Learning sparse graphs under smoothness prior," in *Proc. IEEE Int. Conf. Acoust. Speech. Signal Process.*, 2017, pp. 6508–6512.
- [24] E. Pavez, H. E. Egilmez, and A. Ortega, "Learning graphs with monotone topology properties and multiple connected components," *IEEE Trans. Signal Process.*, vol. 66, no. 9, pp. 2399–2413, 2018.
- [25] H. E. Egilmez, E. Pavez, and A. Ortega, "Graph learning from filtered signals: Graph system and diffusion kernel identification," *IEEE Trans. Signal Inf. Process. Netw.*, pp. 1–1, 2018.
- [26] M. G. Preti, T. A. Bolton, and D. Van De Ville, "The dynamic functional connectome: State-of-the-art and perspectives," *NeuroImage*, vol. 160, pp. 41–54, 2017.
- [27] Y. Kim, S. Han, S. Choi, and D. Hwang, "Inference of dynamic networks using time-course Data," *Brief. Bioinformatics*, vol. 15, no. 2, pp. 212–228, 2014.
- [28] D. Hallac, Y. Park, S. Boyd, and J. Leskovec, "Network inference via the time-varying graphical Lasso," in *Proceedings of the 23rd ACM SIGKDD International Conference on Knowledge Discovery and Data Mining*, 2017, pp. 205–213.
- [29] R. P. Monti, P. Hellyer, D. Sharp, R. Leech, C. Anagnostopoulos, and G. Montana, "Estimating time-varying brain connectivity networks from functional MRI time series," *NeuroImage*, vol. 103, pp. 427–443, 2014.
- [30] J. Wang, S. Qiu, Y. Xu, Z. Liu, X. Wen, X. Hu, R. Zhang, M. Li, W. Wang, and R. Huang, "Graph theoretical analysis reveals disrupted topological properties of whole brain functional networks in temporal lobe epilepsy," *Clinical Neurophysiology*, vol. 125, no. 9, pp. 1744–1756, 2014.
- [31] L. Condat, "A primal–dual splitting method for convex optimization involving Lipschitzian, proximable and linear composite terms," *J Optim Theory Appl*, vol. 158, no. 2, pp. 460–479, 2013.
- [32] K. Yamada, Y. Tanaka, and A. Ortega, "Time-varying graph learning based on sparseness of temporal variation," in *Proc. IEEE Int. Conf. Acoust. Speech. Signal Process.*, 2019, pp. 5411–5415.
- [33] V. Kalofolias, A. Loukas, D. Thanou, and P. Frossard, "Learning time varying graphs," in *Proc. IEEE Int. Conf. Acoust. Speech. Signal Process.*, 2017, pp. 2826–2830.
- [34] B. Baingana and G. B. Giannakis, "Tracking switched dynamic network topologies from information cascades," *IEEE Trans. Signal Process.*, vol. 65, no. 4, pp. 985–997, 2017.
- [35] D. I. Shuman, S. K. Narang, P. Frossard, A. Ortega, and P. Vandergheynst, "The emerging field of signal processing on graphs: Extending high-dimensional data analysis to networks and other irregular domains," *IEEE Signal Process. Mag.*, vol. 30, no. 3, pp. 83–98, 2013.
- [36] N. Parikh and S. Boyd, "Proximal algorithms," *Found Trends Optim*, vol. 1, no. 3, pp. 127–239, 2014.
- [37] R. Tibshirani, M. Saunders, S. Rosset, J. Zhu, and K. Knight, "Sparsity and smoothness via the fused Lasso," *J. R. Stat. Soc. Ser. B Stat. Methodol.*, vol. 67, no. 1, pp. 91–108, 2005.
- [38] L. Meier, S. V. D. Geer, and P. Bühlmann, "The group Lasso for logistic regression," *J. R. Stat. Soc. Ser. B Stat. Methodol.*, vol. 70, no. 1, pp. 53–71, 2008.
- [39] N. Komodakis and J. Pesquet, "Playing with duality: An overview of recent primal-dual approaches for solving large-scale optimization problems," *IEEE Signal Process. Mag.*, vol. 32, no. 6, pp. 31–54, 2015.
- [40] I. Daubechies, M. Defrise, and C. De Mol, "An iterative thresholding algorithm for linear inverse problems with a sparsity constraint," *Commun. Pure Appl. Math.*, vol. 57, no. 11, pp. 1413–1457, 2004.
- [41] P. L. Combettes and J.-C. Pesquet, "Primal-dual splitting algorithm for solving inclusions with mixtures of composite, Lipschitzian, and parallel-sum type monotone operators," *Set-Valued Anal*, vol. 20, no. 2, pp. 307–330, 2012.
- [42] D. B. Johnson and D. A. Maltz, "Dynamic source routing in ad hoc wireless networks," in *Mobile Computing*, 1996, pp. 153–181.
- [43] E. A. Allen, E. Damaraju, S. M. Plis, E. B. Erhardt, T. Eichele, and V. D. Calhoun, "Tracking whole-brain connectivity dynamics in the resting state," *Cereb. Cortex*, vol. 24, no. 3, pp. 663–676, 2014.
- [44] J. Taghia, S. Ryali, T. Chen, K. Supekar, W. Cai, and V. Menon, "Bayesian switching factor analysis for estimating time-varying functional connectivity in fMRI," *Neuroimage*, vol. 155, pp. 271–290, 2017.
- [45] F. Zhang and E. R. Hancock, "Graph spectral image smoothing using the heat kernel," *Pattern Recogn.*, vol. 41, no. 11, pp. 3328–3342, 2008.
- [46] J. Gall, C. Stoll, E. de Aguiar, C. Theobalt, B. Rosenhahn, and H. Seidel, "Motion capture using joint skeleton tracking and surface estimation," in *Proc. IEEE Conf. Comput. Vis. Pattern Recognit.*, 2009, pp. 1746–1753.